12-2016

Printing 3D lithium-ion microbattery using stereolithography

Qiming Chen
Purdue University

Graduate School Form
30 Updated 12/26/2015

PURDUE UNIVERSITY
GRADUATE SCHOOL
Thesis/Dissertation Acceptance

This is to certify that the thesis/dissertation prepared

By Qiming Chen

Entitled

Printing 3D Lithium-ion Battery Using Stereolithography

For the degree of Master of Science in Mechanical Engineering

Is approved by the final examining committee:

Liang (Chair)	Pan
Kejie	Zhao
Justin	Weibel

To the best of my knowledge and as understood by the student in the Thesis/Dissertation Agreement, Publication Delay, and Certification Disclaimer (Graduate School Form 32), this thesis/dissertation adheres to the provisions of Purdue University's "Policy of Integrity in Research" and the use of copyright material.

Approved by Major Professor(s): Liang Pan

Approved by: Jay P. Gore 12/1/2016

Head of the Departmental Graduate Program Date

PRINTING 3D LITHIUM-ION MICROBATTERY USING STEREOLITHOGRAPHY

A Thesis

Submitted to the Faculty

of

Purdue University

by

Qiming Chen

In Partial Fulfillment of the

Requirements for the Degree

of

Master of Science in Mechanical Engineering

December 2016

Purdue University

West Lafayette, Indiana

TABLE OF CONTENTS

Page

LIST OF FIGURES

Figure Page

Appendix Figure

ABSTRACT

Chen, Qiming. M.S.M.E., Purdue University, December 2016. Printing 3D Lithium ion Microbattery using Stereolithography. Major Professor: Liang Pan, School of Mechanical Engineering.

Microbatteries have been gained a lot of importance since the development of micro- and nanotechnologies. Integrating the microbattery system will enable a variety of applications, such as implantable biomedical devices and wireless sensor networks. In this paper, we demonstrated a new method to fabricate three dimensional lithium-ion microbattery using stereolithiography. A UV-curable gel polymer electrolyte resin is first synthesized and characterized. The electrolyte resin is then applied to build into 3D architecture by stereolithography. The gel electrolyte structure is designed into a zigzag shape in order to improve the contact area between electrode and electrolyte. Battery's active material, $LiFePO_4$ (LFP) and $Li_4Ti_5O_{12}$ (LTO), are mixed with the gel electrolyte resin and then flow into the gel electrolyte structure. The result demonstrates a feasibility of lithium-ion microbattery fabricated by stereolithgraphy.

CHAPTER 1. BACKGROUND AND LITERATURE REVIEW

1.1 Introduction

In these last years, many efforts have been devoted to develop autonomous microdevices, such as wireless sensor network, distributed monitors and biomedical implantable devices. In order to ensure a stable or high peak current supply within these microdevices, on-board energy storage is required. The most promising way that guarantees energy storage is using batteries. Also, because of the difficulty to replace batteries within micro-scale, it leads to a demand for rechargeability.

Among all of the rechargeable energy storage system, lithium-ion battery has the highest energy density. It has been widely used in modern technologies. Mobile phones, personal computers and also the electric automotive are equipped with lithium-ion battery. Conventional lithium-ion batteries are based on liquid electrolyte and separator, which limits their design and size. Therefore, building the lithium-ion microbattery becomes one of the leading trends for the microbattery development. Several reviews have reported the latest advance in this field[1-5].

1.2 3D Lithium-ion Microbattery

The thin film lithium-ion batteries (a thickness up to 10μm) have been studied over the last 15 years[6]. However, the limited energy and power available per area of footprint restricts its development. Although the 2D thin film battery can deliver high power, they require large footprints to provide reasonable energies. Making the electrode thicker can theoretically improve the energy density but the resultant increases in electron and ion diffusion length reduce the effective energy and power density.

3D battery architectures are designed to maximize the battery's power and energy density but remain the short ion transport distances. The 3D geometry of electrodes, as shown in Figure 1-1, can potentially double the energy density by fully utilizing the limited space. Compared with the 2D thin film battery, the main advantage of the 3D electrode is the ability to achieve large areal energy capacities without sacrificing power density (increase of area-to-volume ratio in 2D) and/or ohmic potential losses (long ion transport distance in 2D).

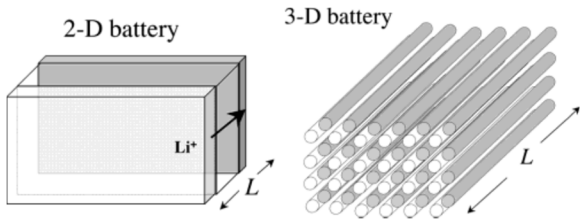

Figure 1-1. 2D parallel plate and 3D interdigitated array batteries.[7]

1.2.1 3D Electrode

2D thin film batteries are assembled by depositing consecutive layers on the same footprint area, which limits the battery's power. On the other hand, 3D batteries are expected to offer a shorter ion transport length and larger areal energy density. As shown in the past review[7], the majority of the 3D battery configurations have relied on the fabrication of electrode/electrolyte materials on 3D micropatterned surfaces, which acts as the mechanical support, separator or current collector. The most common 3D architectures that have been proposed are shown in Figure 1-2.

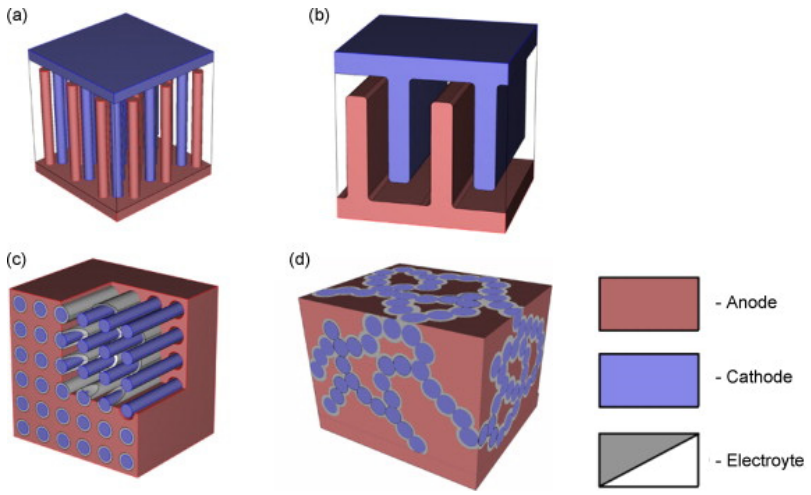

Figure 1-2. Different 3D architectures for microbattery (a) 3D interdigitated, (b) 3D trench, (c) 3D concentric and (d) 3D aperiodic.[1]

3D electrodes can be fabricated using layer-by-layer deposition on a prepared template substrate. Nathan, M., et al.[8]successively deposited five layers onto a high aspect ratio microchannel plate substrate, as shown in Figure 1-3(a). It shows a capacity (1mAh cm^{-2}) much greater than the 2D equivalent. Liu, C., et al.[9]embedded all the battery

components within an anodic aluminum oxide (AAO) nanopore, demonstrated a 1000 cycle life for the microbattery, as shown in Figure 1-3(b). Gowda, S. R., et al.[10] deposited anode (Ni-Sn) and cathode (polyaniline, PANI) nanowires packaged within conformal polymer separator (PEO) using AAO as template, as in Figure 1-3(c). Pikul, J.H., et al.[11] was using holographic lithography to define a 3D lattice on each electrode structure and inverted the structure by nickel electroplating, as shown in Figure 1-3(d).

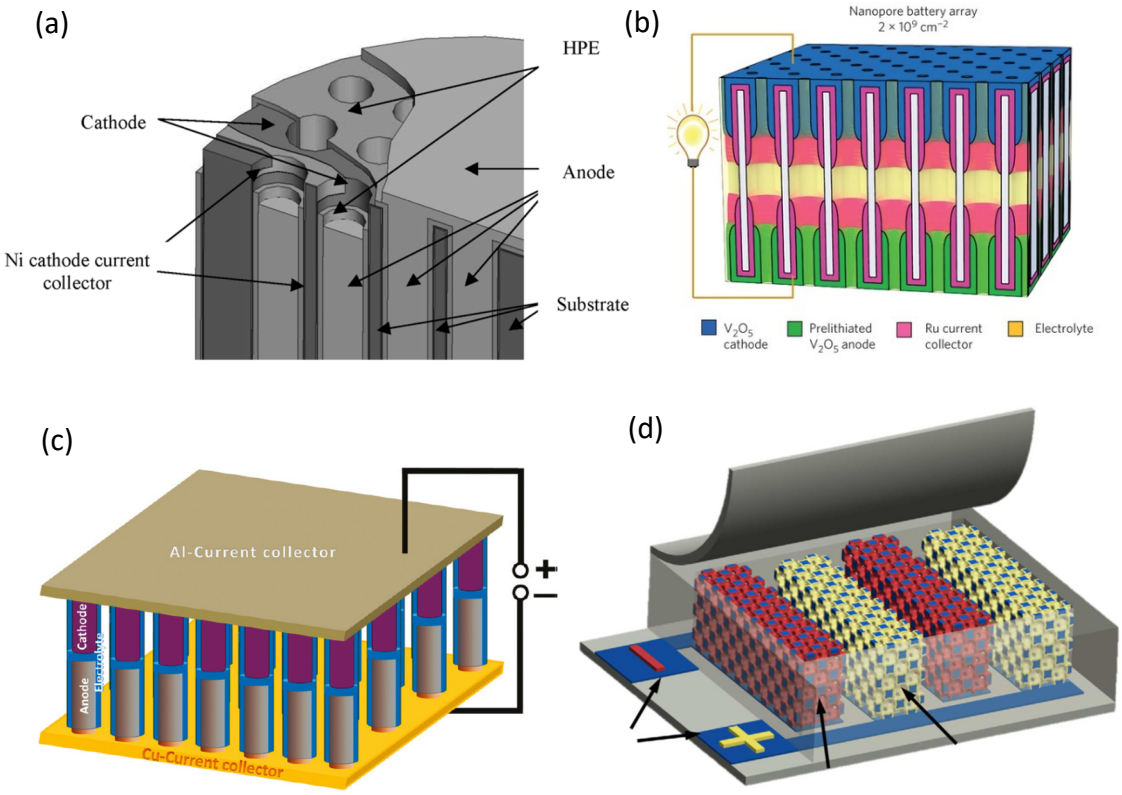

Figure 1-3. (a) Isometric view of the 3D microbattery[8]; (b) cross-section of a single-pore battery[9]; (c) schematic of alumina template based hybrid electrochemical device[12]; (d) nanoporous microbattery electrodes coated on nickel scaffold[11].

There are other papers describing their methods to fabricate 3D microbatteries. Sun, K., et al.[13] built the micro-electrode array layer by layer using the ink jet 3D printer and

achieved a high aspect ratio structure, as shown in Figure 1-4(a). Cheah, S.K., et al.[14] deposited an ALD layer of TiO_2 on Aluminum nano-rods as cathode, testing the 3D electrode in a liquid electrolyte. The result shows a 10 times increase in terms of areal capacity. Wang, C., et al.[15] and Min, H., et al.[16] fabricated microrods based on pyrolized photoresist. The cathodes are selectively grown using electrodeposition, while the carbon rods can be directly used as anodes, as shown in Figure 1-4(b). The result shows the possibility of reversible lithium ion intercalation but with a very large self-discharge in a liquid electrolyte.

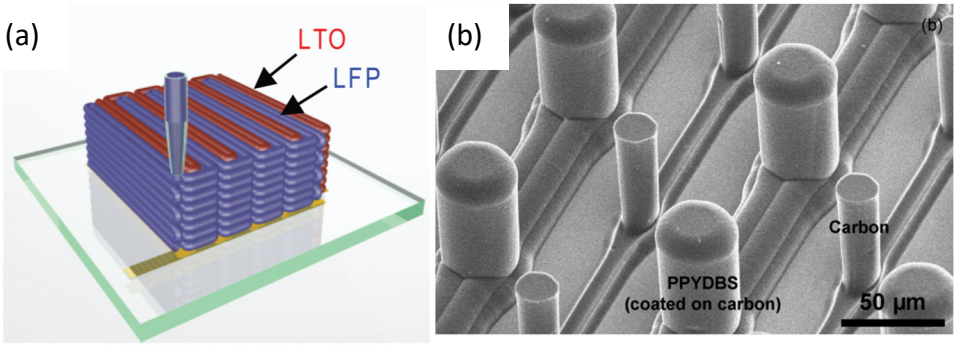

Figure 1-4. (a) 3D interdigitated microbattery architecture fabricated by printing inks through 30μm nozzle[13]; (b) SEM images of C/PPYDBS post array[16].

Among the papers above, electrodes are first deposited and liquid-phase electrolyte is later added as an ion-exchange medium. Because of that, those micro-batteries require sealing cases for containing the liquid, in order to assembly a full cell. Although the liquid electrolyte ensures the micro-battery's electrochemical performance, it still has the potential leakage which leads to safety concerns. Moreover, liquid electrolyte limits

the design of cell structure due to their fluidic characteristic and the require for separator in cell assembly.

1.2.2 3D Solid Electrolyte

Another method to fabricate 3D battery is using solid-state electrolyte. The main advantage for developing all-solid-state microbattery is the avoidance of leakage and more design flexibility due to the lack of separator and sealing case. A honeycomb-structure ceramic electrolyte, as described in Figure 1-5, was prepared by Kotobuki, M., et al.[17]. The electrode particles are fabricated by sol-gel method and injected into the microsize holes of the honeycomb $Li_{0.35}La_{0.55}TiO_3$ (LLT) electrolyte. Zhang, J., et al.[18] fabricated a honeycomb-structure PVDF-based gel electrolyte and exhibited a high conductivity of 1.03mS cm^{-1}. However, they did not make full use of the GPE's 3D structure since they are still using conventional electrode.

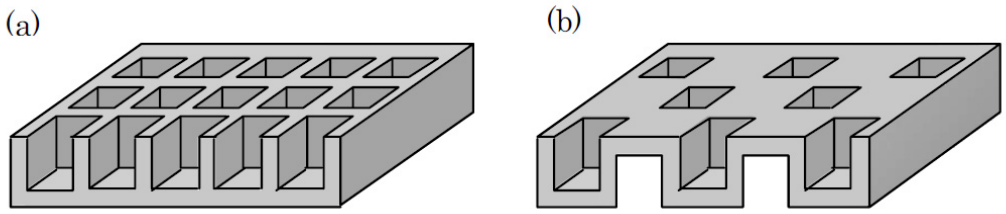

Figure 1-5. LLT solid electrolyte in honeycomb structure: a) structure for half-cell; b) structure for full cell.[17]

The other ways to fabricate 3D solid electrolyte is to cover the 3D electrode with suitable electrolyte layer. Lethien, C., et al.[19] sputtered $LiFePO_4$(LFP)and LiPON as

cathode and solid electrolyte respectively on the Si nanopillars array. Tan, S., et al.[20, 21] reports a self-assembly solid electrolyte with UV-crosslinked poly(propylene glycol) diacrylate (PPO), and the surfactant polyetheramine facilitates self-assembly of the electrolyte onto LFP and Cu nano-pillars. Delannoy, P.E., et al.[22] deposited the silica based ionogel as solid electrolyte onto the electrodes and assembled the full cell battery.

1.3 Solid Polymer Electrolyte (SPE)

The electrolyte is the main component in lithium-ion battery which determines current (power) density, stability and safety of battery. Commercial lithium-ion battery uses liquid electrolyte, absorbed on a porous membrane called separator, which prevents the electrodes from short circuit. However, the carbonate-based liquid electrolytes will undergo deterioration, which not only causes the safety issues (gas generation), but also results in the irreversible reactions with the electrodes (dendrite formation, exfoliation or degradation, etc). The liquid electrolyte requires the sealing of lithium-ion battery and therefore a more complex cell management.

Because of these problems, the research of solid polymer electrolytes (SPE) and gel polymer electrolytes (GPE) has been focused, in order to find an alternative for liquid electrolyte. Moreover, in terms of microbattery, SPE and GPE can also offer a more flexible design and thus a larger energy density.

1.3.1 Lithium Salt

Lithium-ion battery's electrolyte composes of a lithium salt and organic solvents. For the commercial Li-ion battery, $LiPF_6$ is widely used as the lithium salt and DMC-EC are used as solvents. However, the instability of $LiPF_6$ towards ambient moisture restricts its range of applications. The P-F bond is labile towards hydrolysis by even a trace amount of moisture in nonaqueous solvents[23], as illustrated in the following equations:

$$LiPF_6 \leftrightarrow LiF + PF_5 \quad (1)$$

$$PF_5 + H_2O \rightarrow POF_3 + HF \quad (2)$$

Among the products of $LiPF_6$ decomposition, LiF is one of the main components for Solid Electrolyte Interphase (SEI). Another product PF_5 is a strong Lewis acid and tends to react with water. Its product HF will lead to further decomposition of solvents and gas generation, which causes the main safety issue for Li-ion battery explosion.[24]

Among the electrolyte solutes, $LiClO_4$ is another popular choice because of its good solubility and high conductivity. Compared with other salts, $LiClO_4$ has the advantage of less hygroscopic and is relative stable to ambient moisture[23]. Therefore, it is preferred to use for laboratory tests.

Lithium bis(trifluoromethane sulphonyl) imide (LiTFSI) salt is widely used in ionic liquid(IL) electrolyte system. One of the IL, named $(EMI)^+(TFSI)^-$ where EMI^+ is the 1-ethyl-3-methylimida-zolium cation and $TFSI^-$ is bis(trifluoromethane sylphonyl) anion has

been widely studied as a solvent in lithium battery[25, 26]. Adding the lithium salt LiTFSI into it can increase the ionic conductivity which has been reported to be 1.06×10^{-2}S cm^{-1} at 303K[27]. This is close to the organic solvent based electrolyte. LiTFSI salt can also incorporate into the PEO-based SPE system in order to enhance conductivity[28-31]. Its low lattice energy and bulky anions can slow down the recrystallinziation kinetics of PEO-LiTFSI complexes and therefore increase the ionic conductivity[28].

1.3.2 Poly(ethylene oxide) (PEO)

Poly(ethylene oxide) (PEO)/lithium salt complexes is known as solid electrolyte candidate in Li-ion polymer battery since last century[32]. PEO (polyethylene oxide) is a high molecular polymer and its low molecular form is called PEG (polyethylene glycol). Both of the terms refer to an oligomer or polymer of ethylene oxide but PEG is preferred to use in the biomedical field and PEO is more popular in polymer chemistry. Depending on its molecular weight, PEO can be either low-melting solid or liquid.

PEO-based solid electrolyte is the earliest and most studied system. Due to its solubility of lithium salts, PEO has been explored as a suitable matrix for solid polymer electrolyte. The PEO_n-LiX systems can be prepared by solvent casting, hot pressing, lamination, extrusion or even *in situ* polymerization[33]. It has an ionic conductivity which range from 10^{-8} to 10^{-4} at temperature between 40 to 100°C, as shown in Figure 1-6. The relatively low conductivity at ambient temperature prevents it from commercial

application. Because of that, the research of PEO focuses on how to improve its room temperature conductivity.

One approach is to add plasticizer. Ito, Y., et al.[34] and Kelly, I.E., et al.[35] has proven that by adding low molecular weight poly(ethylene glycol) (PEG), which has the same repeat unit as PEO, the conductivity of PEO-based solid electrolyte can reach to 3×10^{-3} S m^{-1} at 25°C and 4×10^{-4} S m^{-1} at 40°C. Ito, Y., et al[34] demonstrated that with increasing PEG content, the conductivity value will also be increased. This is due to the fact that adding PEG can cause an increase of amorphous region which is responsible for the ionic conduction.

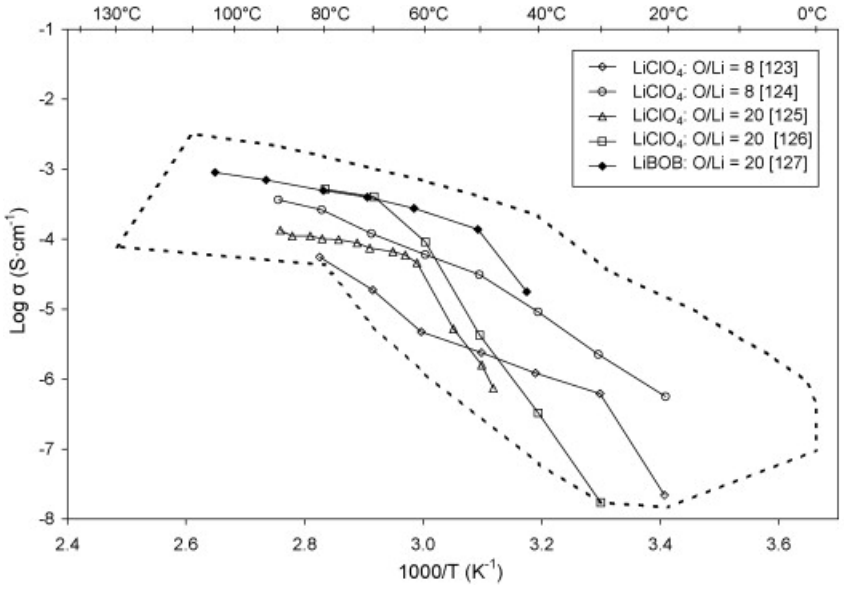

Figure 1-6. Conductivity of PEO with $LiClO_4$ or LiBOB salt.[36]

There are other plasticizers that are reported to increase the amorphous region in PEO, such as, succinonitrile (SN)[37], polysquarate (PPS)[38], lithium

bis(trifluoromethylsulfonyl)-imide (LiTFSI) salt[39] or ethylene carbonate (EC)/propylene carbonate (PC)[40]. However, the absence of crystalline phase results in the decrease of mechanical properties, which makes the SPE less stable.

Adding inert ceramic particles in PEO-based electrolytes is another effective way to improve the thermal, chemical and mechanical stability. It is prepared by mixing a small fraction of micro/nano-size ceramic filler particles, including materials such as Li_3N[41], Al_2O_3[42], SiO_2[43, 44] ZrO_2[45] or TiO_2[46] into the conventional SPE host. As a result of adding fillers into the SPE system, the conductivity has been enhanced by 1-2 orders of magnitude in room temperature. However, a large amount of fillers can cause the degradation of mechanical property.

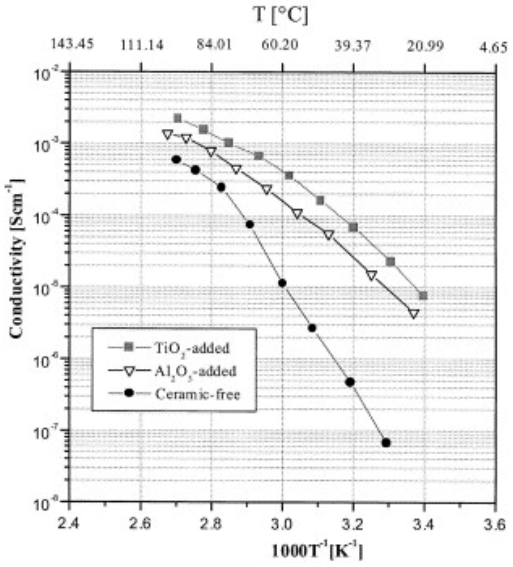

Figure 1-7. log σ versus 1/T plot on $(PEO)_8LIClO_4$ system with TiO_4 and Al_2O_3 fillers.[47]

1.3.3 Gel Polymer Electrolyte (GPE)

GPE is formed by incorporating an organic liquid electrolyte in the polymer matrix. The conducting mechanism in gel electrolyte is similar to that in the liquid electrolytes, but a gel has improved safety and shape flexibility[36]. Tarascon, J.M., et al.[48] employed a poly(vinylidene fluoride)-hexafluoropropylene (PVDF-HFP) copolymer as a matrix to trap the liquid electrolyte. These materials are currently the most used in the lithium polymer battery market. Contrary to the SPE system, ions in GPE move in the liquid or liquid-like phases. Therefore, the conductivity value of near 10^{-3} S cm^{-1} can be obtained with liquid electrolyte/polymer weight ratio higher than 50/50 (w/w)[33]. The conductivity of GPE can be increased by improving the pore structure to facilitate transport of lithium in the solvent. This can be accomplished by incorporating ceramic fillers, as described in PEO-based SPE and modifying the polymer structure. Ren, Z., et al.[49] reported the combination of cross-linked dipoxy polyethylene glycol (DIEPEG) and PVDF-HFP copolymer is one of the efficient way for modifying PVDF-HFP based gel electrolytes. Kuo, C-W., et al.[50] Patal, M., et al.[51] and Perera, K.S., et al.[52] has reported to use poly(acrylonitrile) (PAN) as GPE's polymer matrix. Among the PAN-based electrolyte, the best conductivity is obtained by Patal, M., et al.[51], fabricating GPE with $LiClO_4$ salt and Succinonitrile (SN), with a high value of 7×10^{-3}S cm^{-1}.

The most recent approach in optimization of GPE is to use ionic liquid (IL). IL refers to room-temperature molten salt. Its low toxicity, high thermal stability, low vapor

pressure and flammability make it to be a potential candidate for replacing the organic carbonate solvents in lithium ion battery. Li, Q., et al.[53] fabricated PVDF-HFP electrolyte by incorporating the ionic liquid 1-Ethyl-3-methylimidazolium dicyanamide (EMIMDCA) with a relatively high conductivity (6×10^{-4}S cm^{-1}).

1.4 Flexible and Printable Battery

Recent research has been focused on flexible and printable li-ion battery. The novel designs have enabled batteries that can flex and stretch without significant change in capacity.[54] Although most of them are not built in 3D dimension, their architectures and materials are still good reference for my research. Kwon, Y.H., et al.[55] invented a cable-like flexible battery composed of spiral anode, coated cathode on Al wire, poly(ethylene terephthalate) separator and liquid electrolyte, as shown in Figure 1-8. Koo, M., et al.[56] demonstrated the all-solid state flexible battery packaged by two thin sheets of polydimethylsiloxane (PDMS), which helps the stable settlement of flexible battery, as illustrated in Figure 1-9. Liu, B., et al.[57] fabricated a flexible full battery with 3D nanowire array as anode, conventional coated cathode and liquid electrolyte.

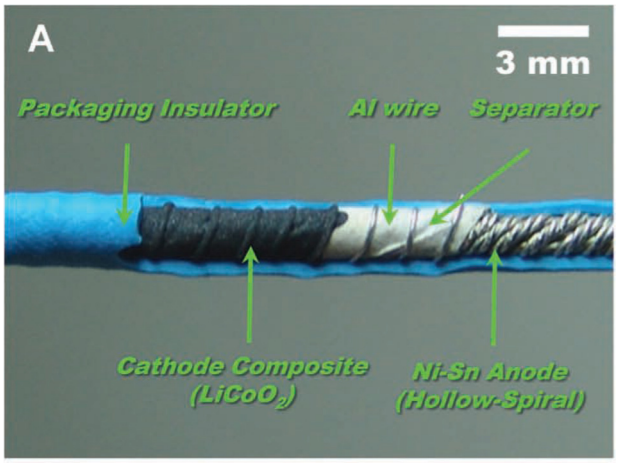

Figure 1-8. Side view of the cable battery separated into component layers.[55]

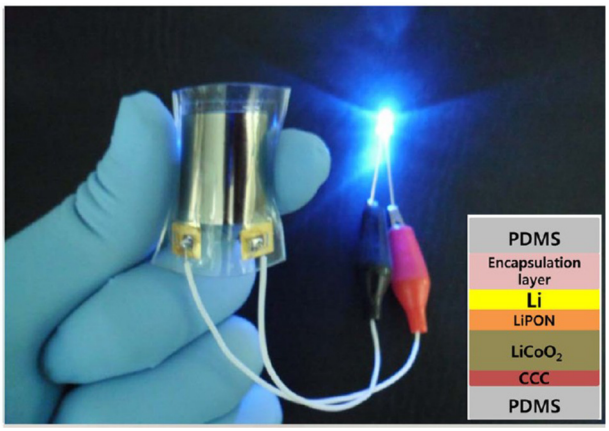

Figure 1-9. Bendable li-ion battery turning on a blue LED in bend condition; inset shows the stacked layer in flexible battery.[56]

Printing process such as screen, stencile, and blade printing can be used to deposit battery components by designing printable inks for the battery's electrodes and electrolyte. Ho, C.C., et al. [58]fabricated 3D zinc-silver microbattery using a custom-built super inkjet printer(SIJP). Sun, K., et al.[13] demonstrated 3D LFP-LTO microbattery with interdigitated electrodes fabricated using custom-built 3D printer. Gaikwad, A.M.,

et al. used stencil printing to deposit the layers for Zn-MnO2 alkaline cells. Kil, E., et al.[59] fabricated a bendable and highly conductive polymer electrolyte using stencil printing followed by UV-crosslinking process.

1.5 Summary

Li-ion battery consists of active layers supported on conductive substrate (current collectors) to form anode and cathode. The electrolyte provides ionic channels between the electrodes. For 3D microbattery fabrication, more researches are focusing on modifying the geometry of electrodes in order to gain more areal energy density. Only a limited number of papers are building the microarchitecture of electrolyte. This is because: 1) the low ionic conductivity for solid electrolyte makes the battery perform worse; 2) the fabrication process for solid electrolyte cannot ensure the shape integrity. In this study, it is proven that we fabricate a well-defined 3D shape gel electrolyte by stereolithography. And the later assembly of full-cell also demonstrated a working microbattery.

CHAPTER 2. MATERIALS AND METHODS

This chapter discusses the materials, fabrication techniques and testing procedures for the microbattery and its components. Section 2.1 and 2.2 provides information about the material and preparation process for gel polymer electrolyte and electrode. Introduction to stereolithography system and the 3D printing process are included in Section 2.3. Microbattery assembly procedure is discussed in Section 2.4. Finally, the processes for material characterization and battery testing are discussed in Section 2.5.

2.1 Gel Polymer Electrolyte

The idea of microbattery fabrication using stereolithography was enlightened by the photo-curable lithium-ion battery material. As stated in other papers, gel electrolyte can be fabricated by incorporating lithium salt into a UV-curable polymer host.[33] Also, electrode can be built into 3D shape by mixing the active material with other UV-curable polymer[60]. Micro-stereolithography can selectively process photo-curable polymers and elastomers into 3D micro-structures at low cost and high speed. We first discuss the material and synthesis of the GPE resin.

2.1.1 $LiClO_4$ Electrolyte

Lithium perchlorate ($LiClO_4$) (CAS number: 7791039, battery grade) (Sigma-Aldrich) is used as the lithium salt in GPE. It has a high ion conductivity (9.0 mS cm^{-1} in EC/DMC at 20°C) and satisfactory solubility. It is relatively stable towards the ambient moisture and therefore a better candidate for lab testing[53]. However, its strong oxidizing property makes it readily react with the organic solvents under high temperature or high current charge.

Ethylene Carbonate (EC) (CAS number: 96491, anhydrous, 99%) and Propylene Carbonate (PC) (CAS number: 108327, anhydrous, 99.7%) are the solvents of $LiClO_4$ salt. Both of them are obtained from Sigma-Aldrich. EC has a melting point (35 – 38°C) higher than the room temperature. However, owing to the suppression by PC, a room temperature melt will be obtained. Also, EC and PC can also be plasticizer for the polymerization.

2.1.2 PEG Resin

Poly (ethylene glycol) Diacrylate (PEGDA) (CAS number: 26570489, average Mn 575), phenylbis(2,4,6-trimethyl-benzoyl)phosphine oxide (CAS number: 162881-26-7) and Sudan I (CAS number: 842-07-9) are obtained from Sigma-Aldrich. The PEG resin using on the micro-stereolithography is composed of 200g PEGDA, 4g phenylbis(2,4,6-trimethyl-benzoyl)phosphine oxide as photo-initiator and 2g Sudan I.

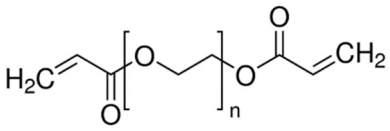

Figure 2-1. Structure of PEGDA olimger.

The photo-polymerization process is illustrated as in Figure 2-2. UV-light can generate radical from photo-initiator, which later reacts with the carbon double chain on PEDGA, and induce the polymerization. This can be used to synthesize PEG hydrogel, which is an excellent candidate for biomaterials.

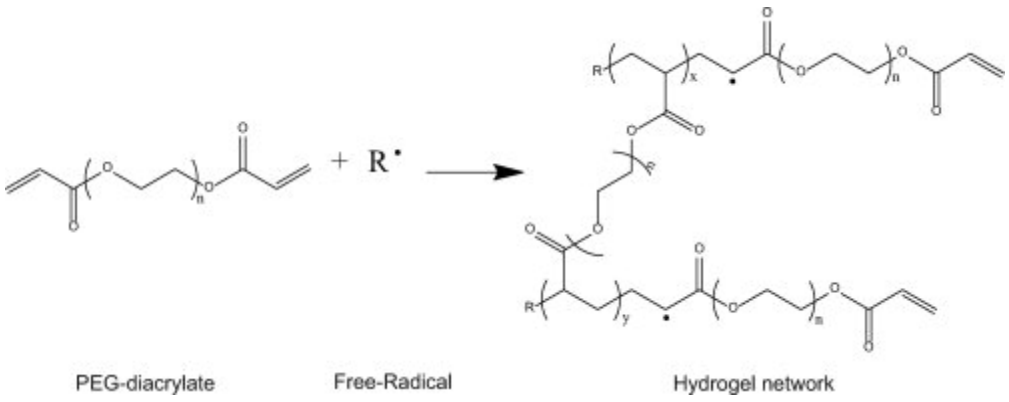

Figure 2-2. UV-polymerization for PEGDA.

2.1.3 Preparation of GPE

GPE composes of 80% (in volume) PEG Resin and 20% LiClO4 Electrolyte. When induced with UV light, the solution will be photo-cured into gel-like polymer membrane. For controlling the thickness of the membrane, aluminum foil, PDMS-coated cover glass and scotch tape are used as illustrated in Figure 2-3. PEG is able to be formed on the surface of aluminum with a native aluminum oxide layer[61]. Also, since the PDMS is inherently

hydrophobic, GPE will be grown on the aluminum surface. Therefore, GPE can be later peeled off from the aluminum for battery assembly.

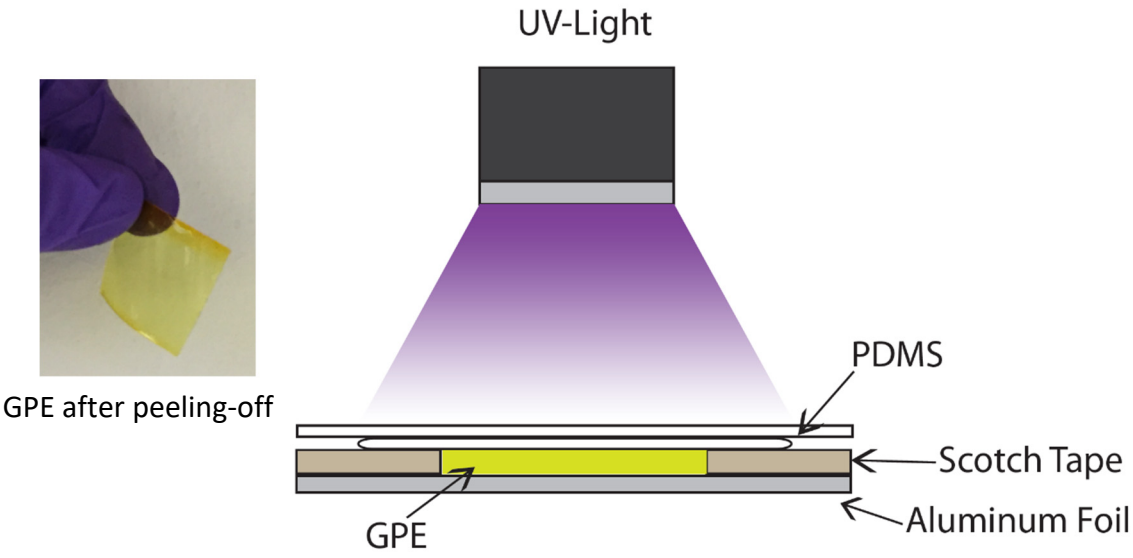

Figure 2-3. Fabrication of GPE.

Scotch tape has a thickness of 80μm. When fabricating the membrane, three tapes are stacked together in order to achieve a thickness of 240μm. The thickness can be varied due to the deformation of the tape. Therefore, the membrane's thickness will be measured again after fabrication.

2.2 Electrode Mixture

For accommodating the 3D shape of GPE, the conventional slurry-cast method for manufacturing solid electrode cannot be applied. Electrode mixture composed of the

active material, carbon black and GPE resin. Carbon black ensures the electrical conductivity, while the GPE resin provides the ionic channels for active material.

2.2.1 LFP and LTO

$LiFePO_4$ (LFP) and $Li_4Ti_5O_{12}$ (LTO) are purchased from MTI Co. and applied as battery's active materials. LFP has a particle size(D90) of <15μm and LTO of 4.24μm (D90). The LFP/LTO redox couple has a benefit of solid electrolyte interphase (SEI)-free, since their potential vs. Li/Li^+ are lower than the formation of SEI. Moreover, due to the strong oxidization, $LiClO_4$ electrolyte cannot be used for cathodes that have a redox activity at potentials higher than 4V vs. Li/Li^+. Therefore, we choose LFP (3.5V vs. Li/Li^+) as cathode material and LTO (1.55V vs. Li/Li^+) as anode. Furthermore, Al can be also used as current collects for both electrodes in LFP/LTO battery.[53, 62]

2.2.2 Mixture with GPE Resin

The electrode mixture is composed of active materials (LFP/LTO), carbon black and GPE. The Super P® Conductive Carbon Black is obtained from MTI CO. Its BET Nitrogen surface area is 62 m^2/g. Adding GPE into the electrode material can provide ionic path for active material and thus increases the ion conductivity. On the other hand, carbon black improves the electrode's electronic conductivity. The resultant LFP and LTO mixture is composed of 0.76g LFP, 0.016g CB, 1.1mL GPE and 0.76g LTO, 0.016g CB, 1.3mL GPE.

Figure 2-4. Electrode mixture.

2.3 Microbattery Assembly

GPE is built into 3D shape using micro-stereolithography. Electrode mixture is then flow-in into the GPE structure. Current collectors are placed for microbattery's test. The assembly process are shown below:

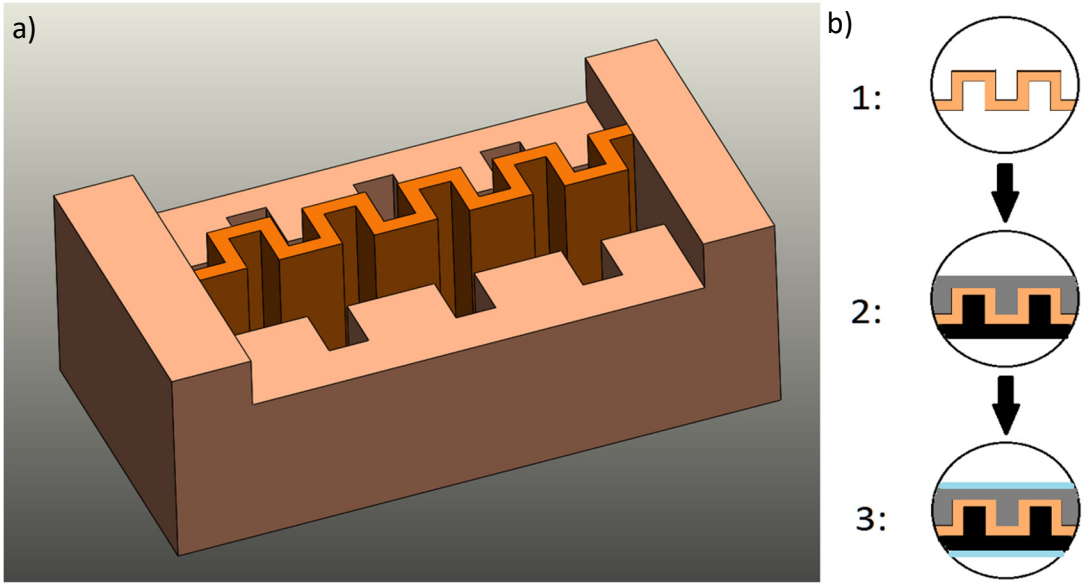

Figure 2-5. Microbattery's geometry and assembly: a) 3D geometry of GPE structure; b) microbattery assembly process: 1. fabrication of 3D GPE; 2. flow-in of electrode mixture; 3. inserting current collectors.

2.3.1 Stereolithography System

The SLA system we built composes of three modules: 1) the motorized translation stage, 2) optical systems and 3) Digital Micromirror Device (DMD). The translation stage is obtained from PI and has a resolution of 50nm. During fabrication, it moves downwards to create rooms to let resin flow in for new layer. As seen in Figure 2-6, fresh resin is held by the surface tension between cover glass and silicon substrate, which increases the uniformity for new layer. The cover glass is spin-coated with Polydimethylsiloxane (PDMS). That is because solid polymerized PDMS will present an external hydrophobic surface, which facilitates the release of newly-built layer after curing. However, it will also cause problems such as bubble generation, limited aspect ratio and peeling-off of structure from the substrate. The pattern irradiated on the top of cover glass is predefined by the DMD mask. The maximum footprint for current configuration is 12.6mm by 7.1mm. The maximum footprint area can be increased by adjusting the lens configuration, with a trade-off of lower resolution.

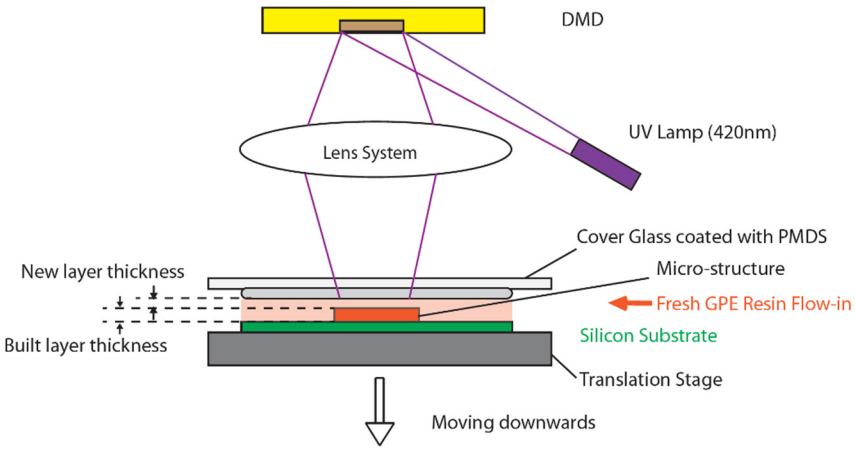

Figure 2-6. Micro-stereolithography system.

2.3.2 3D Microbattery Assembly

The 3D structure is first designed using Solidworks and exported as a STL file. The part is then sliced into layers in order to be used by stereolithography. The structure has a footprint area of 7.6mm by 3.8mm, with a height of 3mm. Two trenches are home to the current collectors as well as the electrode mixture material. The center membrane is acting as the battery's gel electrolyte and is designed into a zigzag shape in order to increase the contact area between electrode and electrolyte. The thickness of the membrane is 200μm. It is so thin that deformation will happen during fabrication. Therefore, the side walls located at the two ends of center membrane are used to hold the membrane and ensure it to be vertical and completed.

The three cuts on the trench side provides a channel for electrode mixture flowing in. The center membrane is higher than the sides for preventing the electrode mixture from overflow to the other side. Moreover, since the GPE is soft and brittle, the base of the structure has to be large enough to hold the upper part. Otherwise, the thin wall will collapse when it is too high.

After fabrication, by stereolithography, the structure is rinsed by IPA and dried using air gun. Adequate amount of electrode mixtures are flown into the trench, as shown in Figure 2-7(b). The SEM pictures, as seen in Figure 2-7(a), (c) and (d) shows the 3D GPE structure and the polymer chain structures.

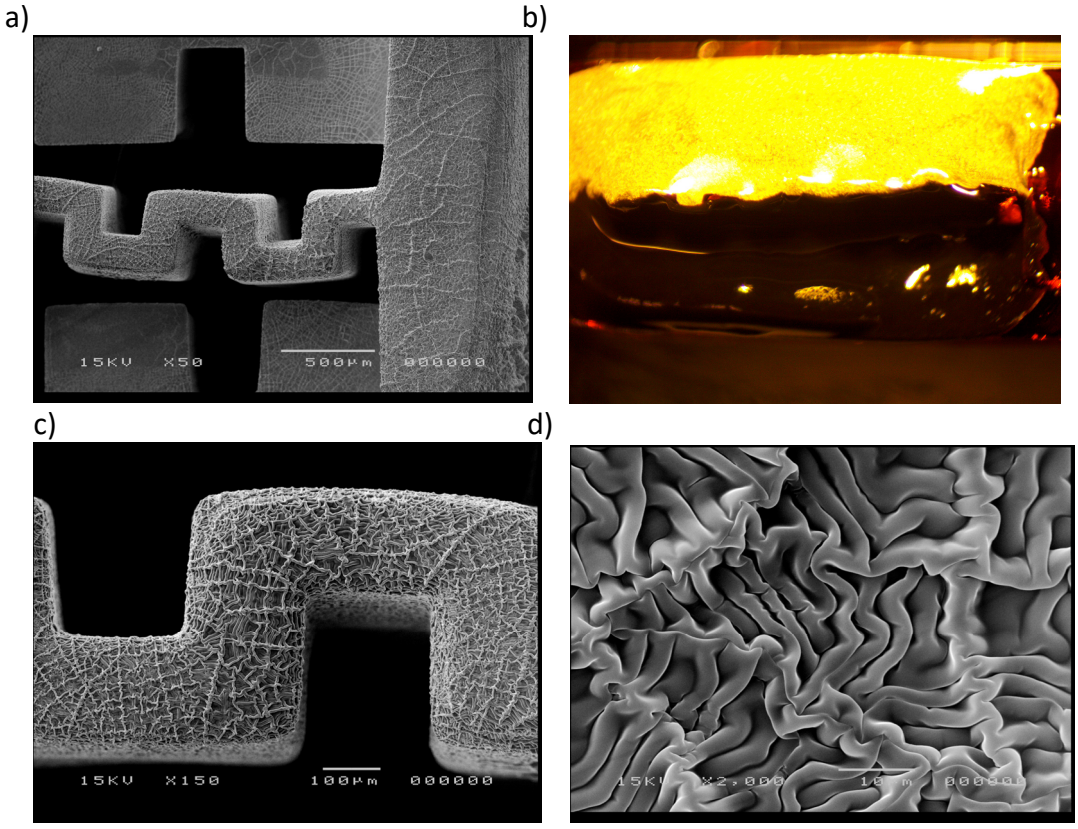

Figure 2-7. Microbattery assmbly process: a) SEM picture of 3D GPE structure fabricated by stereolithography; b) after filling the trench with electrode mixture; c) SEM picture of Zigzag structure d) polymer matrix in 3D GPE.

As shown in Figure 2-7(d), the PEG matrix has the pore size in nano-scale, which indicates the lithium ion channel in the gel electrolyte. The pores facilitate the ion transport in GPE.

2.4 Battery Testing

2.4.1 Ion Conductivity

The ion conductivity is measured using Electrochemical Impedance Spectrum (EIS). A holder was made by Makerbot using ABS. Since the GPE consists of organic solvents (EC

and PC), it will dissolve ABS. Therefore, we treat the surface of ABS holder by coating a layer of UV-cured PEG resin.

A spacer is first taped onto the top of the center square on top part. Cooper foils are cut for the electrical connection. Aluminum cannot be used here because it will influence the measurement result. Two spacers are then inserted into the circle hole on bottom part. After placing the cured GPE membrane onto the center, the two parts are closed and fixed by four screws and nuts through the corner holes.

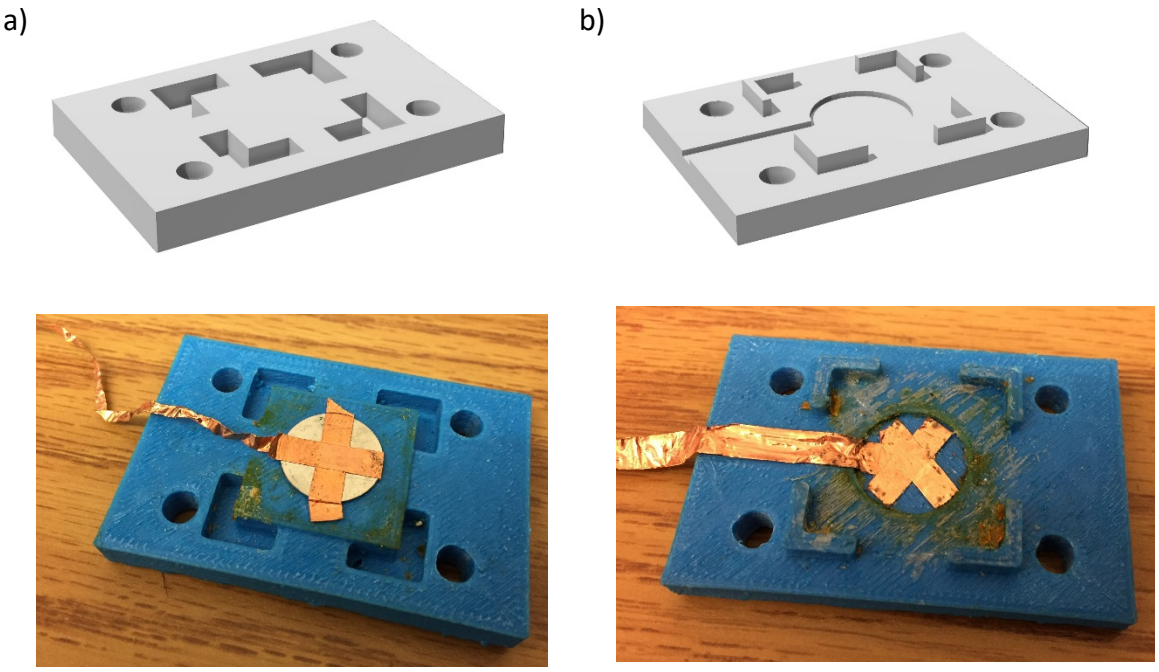

Figure 2-8. Holder (left: top part, right: bottom part) for GPE's EIS measurement.

2.4.2 GPE Characterization

LFP/GPE/Li are assembled for characterizing the cycle performance of GPE. Liquid electrolyte ($LiClO_4$(PC+EC)) is used to wet the cathode and anode material. GPE is fabricated, punched into a circle and then placed between cathode and anode. The coin

cell is crimped with spacer and spring for ensuring the contact. The cycle test is then performed on Arbin AT-2000.

Another simple way to test the GPE is to stack the battery layer and fix with two cover glasses and clips. As shown in Figure 2-9, the electrode and electrolyte layer are fixed by clips and cover glasses. Potentiostatic charging is applied. The battery can turn on a LED for minutes.

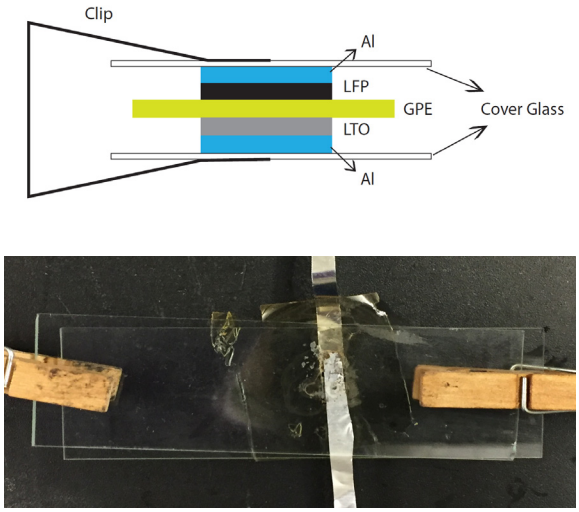

Figure 2-9. GPE test with stacked battery layer.

2.4.3 Mircobattery Cycle Test

Since the microbattery cannot be fitted into the conventional battery testing platform. We use multimeter to perform cycle test for the microbattery, as seen in Figure 2-10. Ammeter is placed in series with the power supplier and microbattery. A voltmeter is connected in parallel to measure the battery's voltage. The charging and discharging process is manually controlled by a switch. While charging, the power supplier will

provide a 4.2V voltage to the microbattery. Ammeter's reading is recorded every 1 minute. At the discharging step, the microbattery is connected to a small red LED. The reading is still recorded every 1 minute.

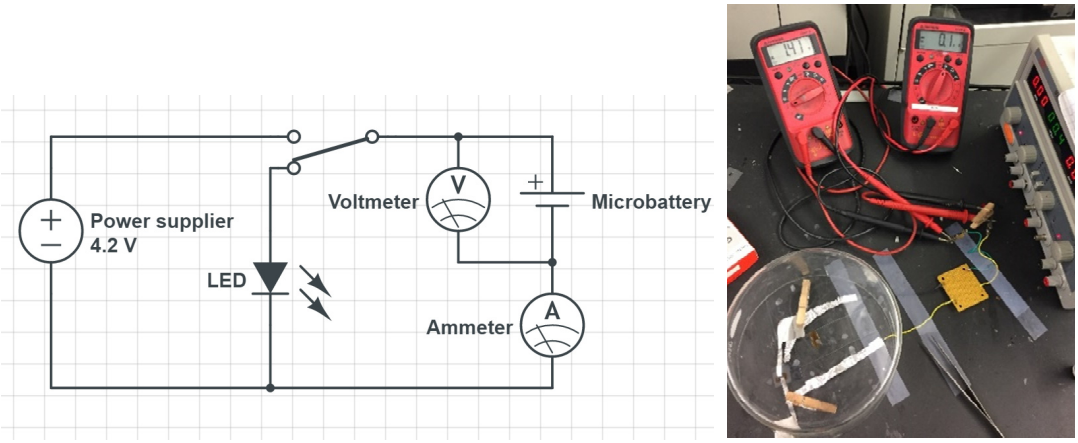

Figure 2-10. Microbattery cycle test setup.

CHAPTER 3. RESULTS AND DISCUSSIONS

3.1 Electrode Mixture

For accommodating the 3D geometry of the GPE, we need to find a solution to build the electrode into 3D as well. Electrode mixture is created only for proof-of-concept's purpose. Active material, conductive carbon black and GPE resin are mixed to form an electrode material. The carbon black proves the electrical conductivity, while GPE resin provides ionic channels for the active material.

3.1.1 Rheology Control

Controlling the rheology of electrode mixture is important for microbattery assembly because we need to fill the trench with the electrode mixture. The viscosity of electrode mixture is tailored by changing its composition ratios. It is reported that adding more solid contents (LFP/LTO powders and carbon black (CB) additives) will cause agglomeration of particles in electrode mixture and reducing the content will weaken the thixotropic fluid characteristic[62]. However, in our experiment, we found that it is the content of carbon black which majorly influences the slurries' rheology.

By adding carbon black into the mixture, the solution is becoming more viscous. We start from a composition of 1.0ml PEG, 1.0ml LiClO4 (PC + EC), 0.27g LFP powders. It has a low viscosity and cannot maintain on a vertical aluminum foil. After adding 0.015g CB (5% in mass of solid) into the mixture, its viscosity is increasing dramatically, as you can see from the figure. Keep adding carbon black can make the viscosity even higher.

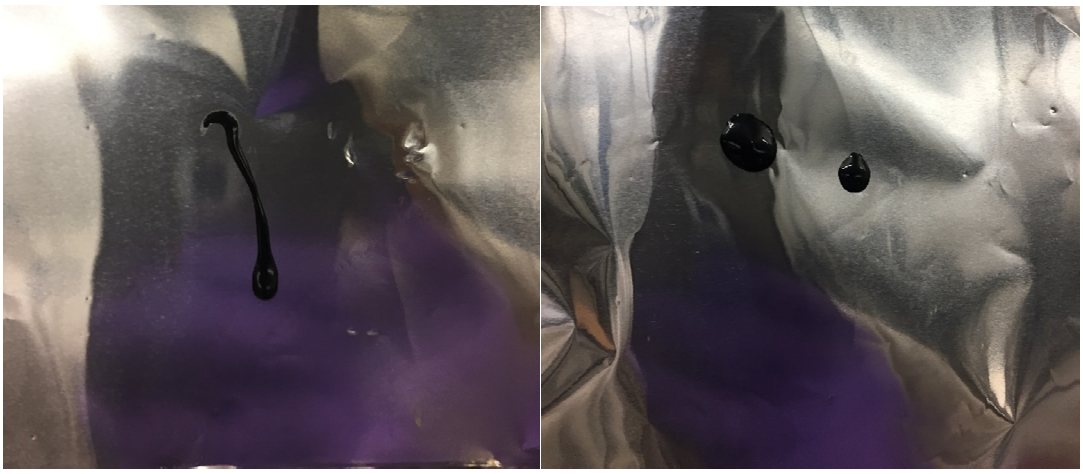

Figure 3-1. Fluid characterization for electrode mixture with different CB content (Left: 0%, Right: 5%).

3.1.2 Electrode Photo-curing

The electrode composes of GPE resin and solid contents (LFP, LTO and CB). When exposed the electrode mixture to the UV irradiation for a short time, the mixture will be photo-cured and form a GPE matrix-embedded gel-state electrode. It is demonstrated that with the UV-curing process, the electrode mixture will have better conductivity and better performance, due to the good dispersion of material[62]. As shown in Figure 3-2,

the cured LFP and LTO mixture can form a membrane with a thickness less than 100μm. Since the curing depth is too small, it is difficult for it to be applied on microbattery.

We can also do thermal curing for LFP/LTO mixture in order to make gel-state electrode. However, when doing the thermal curing, the hot plate temperature must be higher than 100℃. The liquid content inside GPE will be evaporated during the heating process. Therefore, when thermally curing, the GPE micro-structure will shrink and deform, which destroys the microbattery.

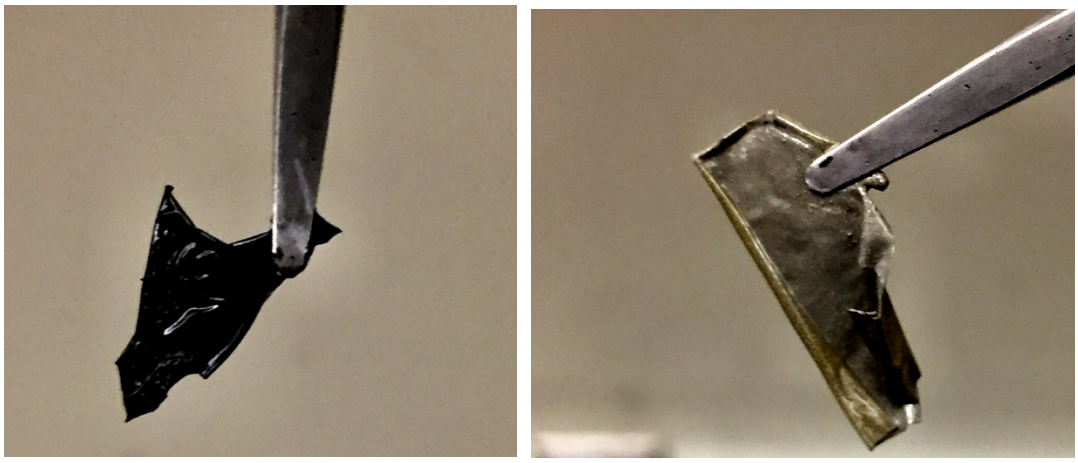

Figure 3-2. Electrode mixture after photo-curing (left: LFP, right: LTO).

3.2 Gel Polymer Electrolyte Fabrication

3.2.1 Adding Al_2O_3 Nanoparticles

As described in previous articles[63-66], the nanoparticles filler can increase the ion conductivity and mechanical stability of polymer electrolyte. we mix 1ml GPE with 2g Al_2O_3 nanoparticles. After photo-curing, we get a membrane with a thickness around

160µm. The curing depth is becoming smaller but the mechanical integrity increases. The film is not transparent anymore, rather it appears to be yellowish. We then assembled a battery with the photo-cured electrodes and got a working battery.

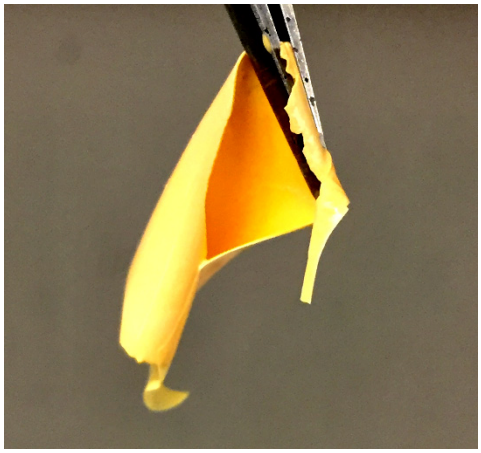

Figure 3-3. PEG mixed with Al_2O_3 nanoparticles after photo-curing.

3.2.2 Various 3D Structures

Different 3D structures have been made on the stereolithography. These include the structures those were not successfully fabricated or assembled. Detailed analysis is provided as below:

1) Microfluidic Channels

   Two channels will be flow in the different electrode materials separately. Electrode slurries will be filled from the inlet openings on the top. A filter paper (pore size of several micros) is placed at the outlets on the side until the channels are filled by the material. The filter paper can ‘drag’ the liquid along the channel and leave the solid

content inside the channels. The wall between channels acts as an GPE membrane. Finally, the current collectors are placed at the inlet openings.

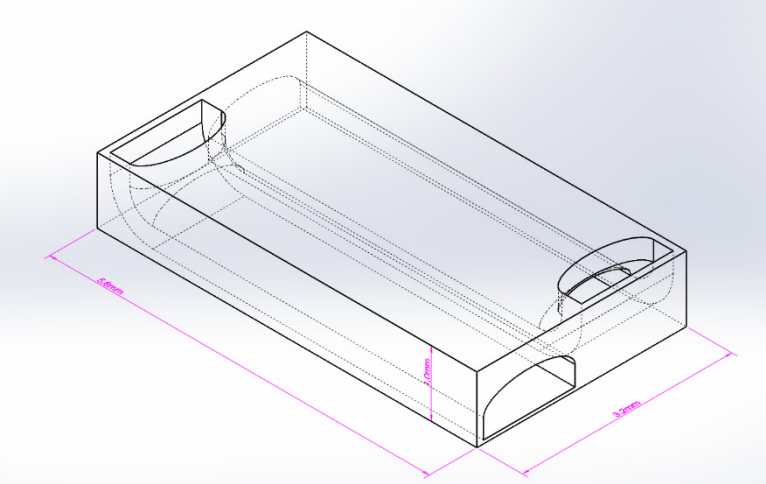

Figure 3-4. Microfluidic channel structure A.

This structure failed to be fabricated at the first several attempts. The major reason for the fabrication difficulty is that the cured GPE is too soft to support the channel structures. The channels will therefore be collapsed and blocked. Moreover, due to the elbow structure of the channel, the mixture tends to be accumulated at the elbow and cannot get to the outlet.

Another structure, as shown in Figure 3-4, is similar to the first one. They are all in a shape of channels with inlet and outlet but the second one has more channels than the first one. The inlets for cathode and anode materials are faced to different directions, which prevents the accidentally mixed when filling. The structure also

faces the same fabrication difficulty as the first one but the slurries are able to reach the outlet.

However, it gave rise to another issue, that is, the liquid part of electrode material is adsorbed by filter paper, leaving some of the solid content adhered to the channel walls. The filter paper also adsorbs some of the solids. Continuingly adding the electrode mixture cannot fill out the entire channels. It leaves a hollow part inside the channel and uneven distribution along the channel wall. Therefore, the idea of using a filter paper is given up.

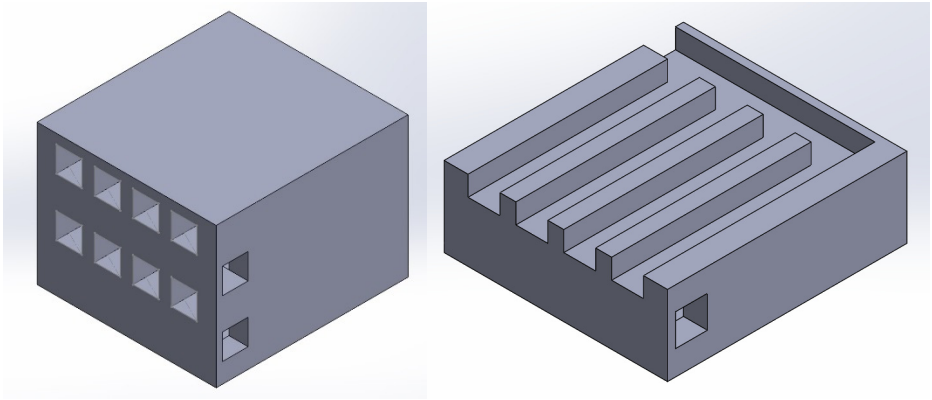

Figure 3-5. Microfluidic channel structure B (left: entire model; right: cross-section).

2) Fin Structure

Fin structure has the benefit of resting the electrode material into each pouch (the fin feature). As shown in Figure 3-5, the electrode slurries are flowed-in from different inlets (the 4 square openings at the side) and will be trapped within the fin

structure. The GPE wall between neighboring fins act as the ion-exchange membrane for battery. Finally, gold is sputtered on the inlet.

The fin structure traps the electrode material very well. However, the sputtering result is not good enough to form a continuous gold metal layer. It is believed that the gold layer is not uniformly covered inside the channels as well as the inlet openings. Also, the gold layer is so thin that it will be moved out by even a gentle touching, which makes it difficult for the microbattery testing.

Moreover, for avoiding the use of filter paper, we also designed a structure without any openings as an outlet. Therefore, it requires a vacuum pump to push the electrode mixture inside the fins. However, the attempt failed because while vacuuming, the trapped air inside the channels is pushing the mixture material and eventually blow away the electrode.

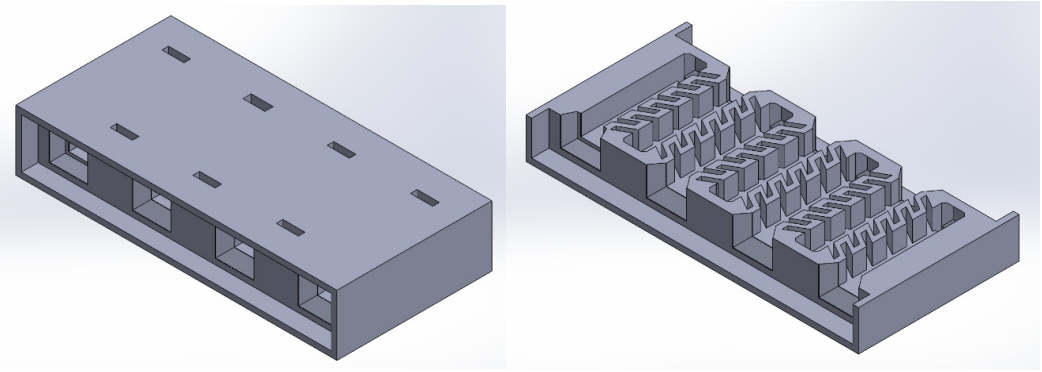

Figure 3-6. Fin structure (left: entire model; right: cross-section view).

3) Wall Structure

We finally get to the wall structure as illustrated in Figure 3-7. Owing to the extruded structure, it is relatively easier to fabricate (no overhung feature) and good enough for proof-of-concept application. To build the structure as tall as possible can facilitate later inserting and keeping the current collectors within the trench.

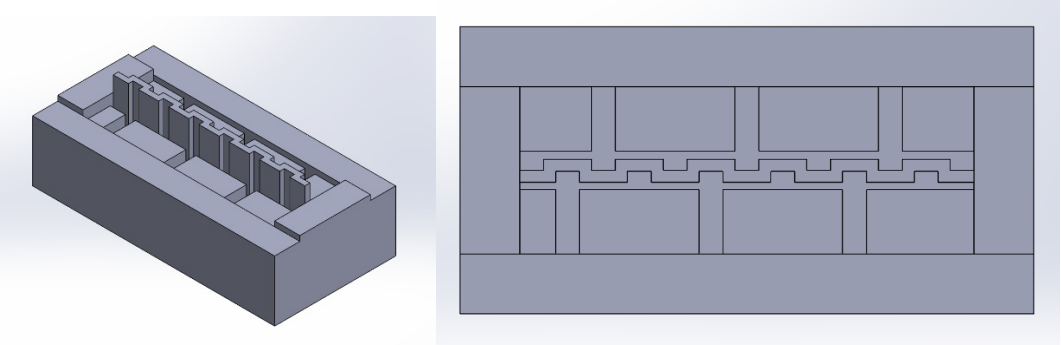

Figure 3-7. Vertical wall structure (left: entire model; right: top view).

3.3 Material Characterization

GPE is characterized using Electrochemical Impedance Spectroscopy(EIS) and cycling measurement platform Arbin AT-2000. Ionic conductivity is first measured for determining the adequate liquid amount within the GPE. Cycle test is then performed on LFP/GPE/Li for achieving the cycle performance of GPE.

3.3.1 Ionic Conductivity Measurement

EIS measurement is conducted with the assistance of Rong Xu in Prof. Zhao's lab. As shown in Figure 3-9, the ionic conductivity increases with the increasing ration of electrolyte solution. This validates that, the liquid electrolyte $LiClO_4$ (EC+PC) can perform

as a plasticizer in polymerization. Therefore, it provides more amorphous region for ionic conduction. The samples are prepared into four groups. Each of them consists a mixture between liquid electrolyte and PEG resin with different volumetric ratio. The ionic conductivity is then calculated as below:

$$\sigma = {R_l}^{-1}A^{-1}\mathrm{t} \tag{3}$$

where t is the thickness, R_l is the intercept between the curve and real axis, and A is the surface area of stainless steel.

The calculated ionic conductivities are 1)4.8E-3S·cm^{-1}, 2)1.3E-3S·cm^{-1}, 3)2.0e-4S·cm^{-1} 4)8.2e-6S·cm^{-1}. The conductivity is decreased with a decreased amount of liquid electrolyte. This demonstrates the less amorphous region in GPE, where the ion can pass easily. Also, when observing the GPE membrane's mechanical property, the more liquid electrolyte it contains, the softer the membrane is.

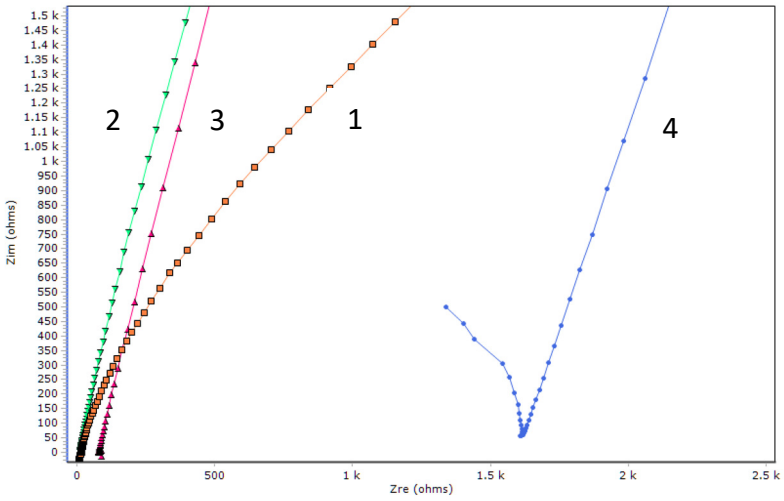

Figure 3-8. EIS Measurement for different compositions of GPE: 1) 80% Electrolyte; 2) 60% Electrolyte; 3) 40% Electrolyte; 4) 20% Electrolyte.

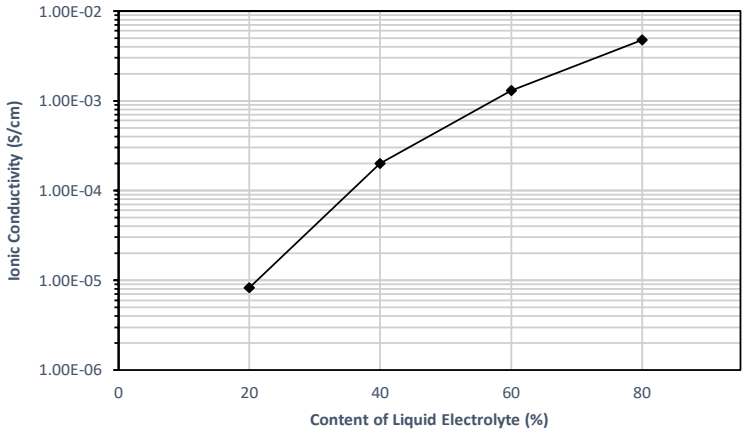

Figure 3-9. Ionic conductivity for GPE with different amount of liquid contents.

3.3.2 GPE Cycle Test

A half-cell is assembled to test the cycle performance of GPE. LFP/GPE/Li coin cell is assembled inside a glovebox and then tested on Arbin. A slow charging rate (C/20) is applied first. The result shows a clear charging plateau around 3.5V (Li/Li^+) and discharge plateau around 3.4V, which is the theoretical value of LFP. The coulombs efficient is of 97.7%. The resultant cycle diagram is shown as below.

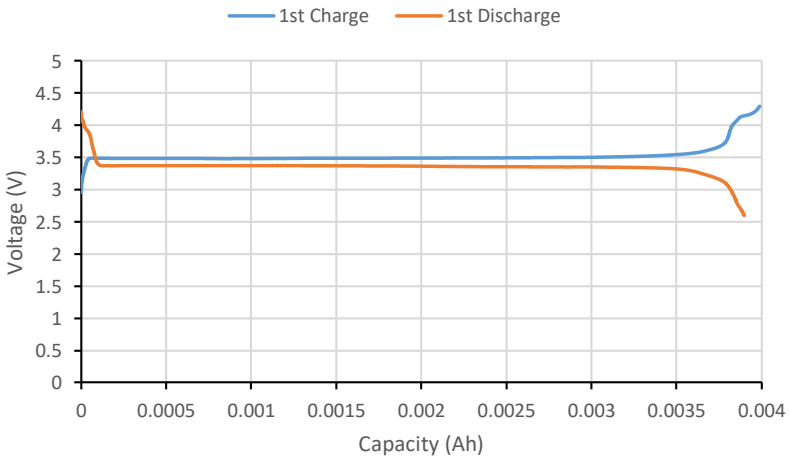

Figure 3-10. Cycle test for LFP/GPE/Li Coin Cell (C/20).

Further cycling test is continued using a higher charging current (C/5), as shown in Figure 3-11. The capacity has a slightly decrease in the second and third cycle, and drops suddenly to near 40% in the fourth cycle. And it appears that the GPE is failed at the 10th cycle. This result is different than the other papers, in which a similar fabrication method is applied for the cross-linked gel polymer electrolyte[67, 68].

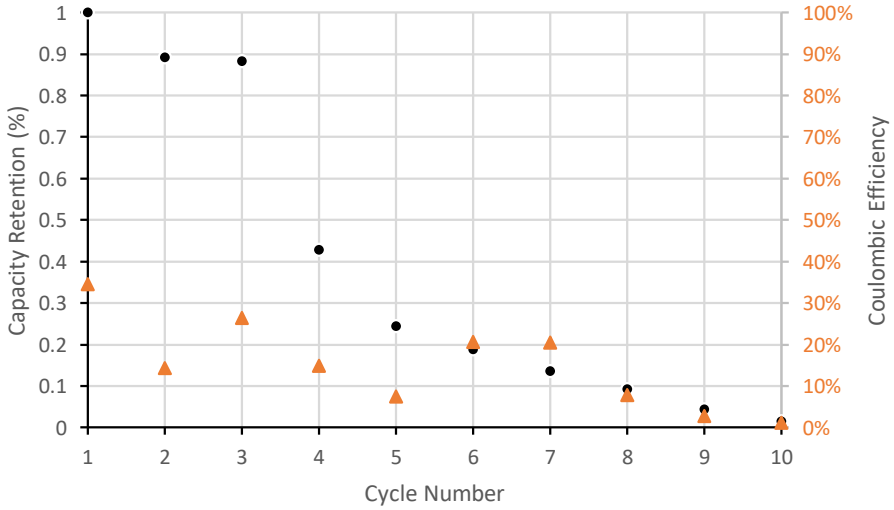

Figure 3-11. Capacity retention vs. cycle number for LFP/GPE/Li coin cell (C/5).

3.3.3 Electrode Mixture

Due to the 3D architecture of our gel electrolyte, a shape-flexible electrode should be fabricated in order to increase the contact area between electrode and electrolyte. Therefore, the active material is mixed with GPE resin to increase the ionic conductivity and carbon black to increase the electronic conductivity. The material is only for proof of concept purpose and not ideal for the real application.

For testing the feasibility of electrode mixture, we stacked the LFP-GPE-LTO layers and assembled a coin cell battery for testing the material. The charging current is set to be 50μA which is 10 times higher than the discharing current, 5μA.

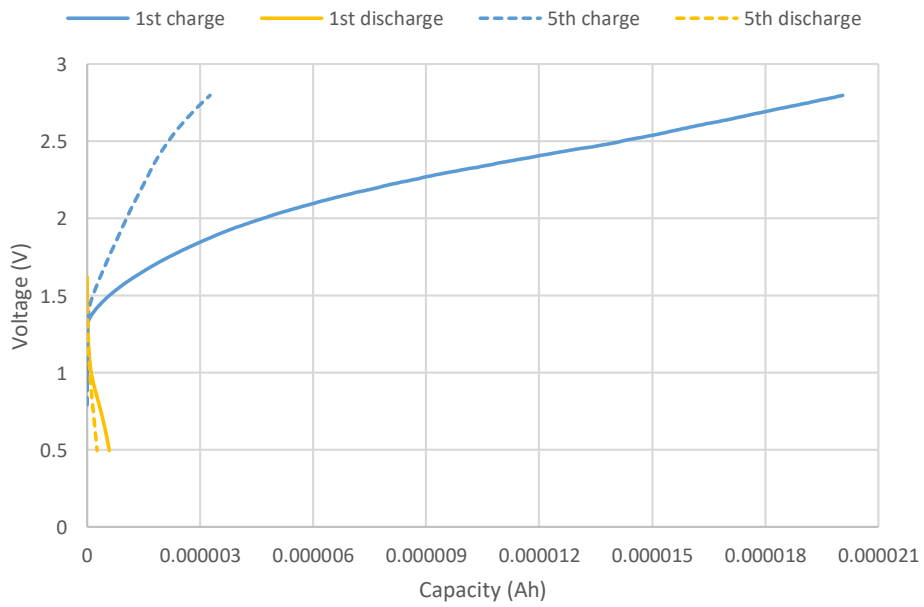

Figure 3-12. Cycle test for LFP mixture/GPE/LTO mixture.

The result in Figure 3-12 shows a positive conclusion for electrode mixture to be used as a proof-of-concept material. However, no apparent charging and discharging plateau is observed on the cycle curve. Also, the discharging voltage is lower than the ideal LFP/LTO redox couple. This is possibly because of the larger electronic resistance caused by the GPE resin in electrode mixture. Also, the discharging capacity is decreased as cycle number increases. The possible explanation to that the build-up of internal resistance during the cycle test lower the performance of the battery.

3.4 Cycling Test for Microbattery

The microbattery is tested using multimeter. It is charged potentiostatically and discharged by powering a small LED. The result is shown as below. Two charge-discharge cycles are observed and it shows an areal energy density of 1.4 μAh/cm^2.

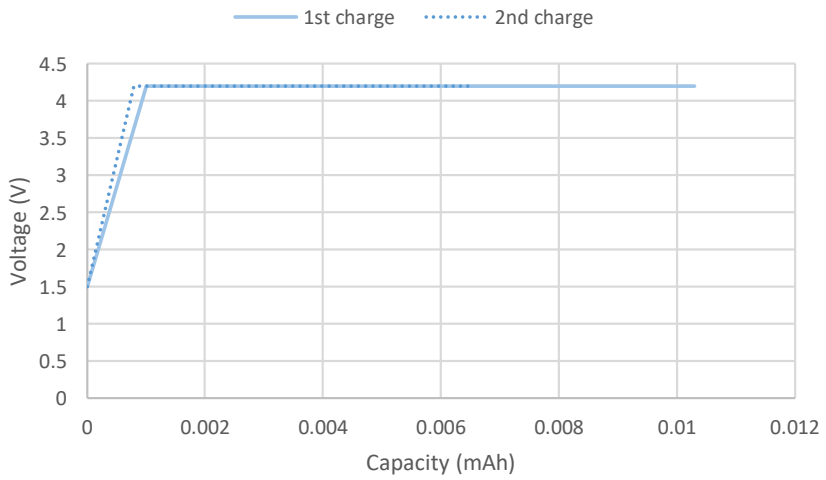

Figure 3-13. Potentiostatic charging process for microbattery cycle test.

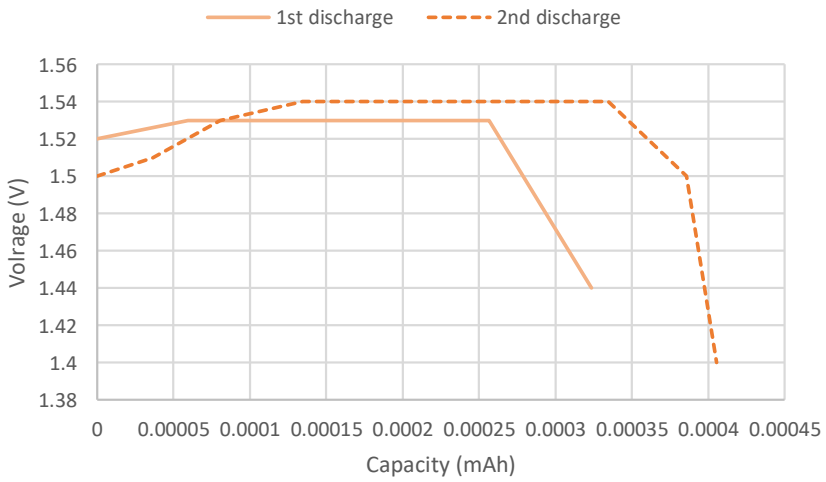

Figure 3-14. Discharging process for microbattery cycle test.

Through theoretical calculation, the surface area for the zigzag membrane is 27.9mm^2. Based on the capacity (0.004Ah) we got from the GPE characterization, the theoretical capacity for microbattery is 0.725mAh. Therefore, for the areal capacity, the theoretical value is 2.51 mAh/cm^2. This is about 2000 times difference between the measured value.

The main reason is the use of electrode mixture, which causes a large internal resistance inside the microbattery and consume a large amount of energy. Moreover, this is possibly due to the out-of-glovebox fabrication process for the microbattery, which will cause the reaction between air or moisture and the battery's components. It is observed that during the microbattery's charging process, some bubbles are generated in the anode side. It is followed by the disappearance of the liquid content. Since PC and EC are high volatile organic solvent, it is concluded that certain chemical reaction is happened during the microbattery charging process. On the other hand, since the electrode mixture characterization is performed in argon-filled coin cell environment, the cycle performance is better than the microbattery.

CHAPTER 4. CONCLUSIONS

Micro-stereolithography has been successfully applied in fabrication of the gel polymer electrolyte in 3D lithium-ion microbattery. The result shows a feasibility to manufacture 3D microbatteries in a low-cost and high-yield method.

UV-curable PEO-based GPE membrane is fabricated and characterized. The GPE membrane shows a high ionic conductivity in room temperature. The ionic conductivity will be increased with the increasing amount of liquid content in GPE resin. It also shows a few successful cycles in half-cell test.

The 3D GPE structure is then built by stereolithography. The microbattery structure we created has an advantage of no liquid leakage compared with other's works. Moreover, stereolithography can create arbitrary architectures for GPE, which facilitates the optimization for microbattery's areal capacity as well as the contact area between electrode and electrolyte.

After the microbattery assembly, cycle test has been performed to show a successful operation for 2 cycles under potentiostatic charging condition, with a measured specific capacity of 1.4 $\mu Ah/cm^2$.

Future work for this topic should be focused on increasing the cycle performance for the GPE membrane and microbattery. The GPE's recipe should be modified to increase both its mechanical and electrochemical prosperities. Also, 3D solid electrode needs to be manufactured in order to reduce the internal resistance.

LIST OF REFERENCES

LIST OF REFERENCES

1. Ferrari, S., et al., *Latest advances in the manufacturing of 3D rechargeable lithium microbatteries.* Journal of Power Sources, 2015. **286**: p. 25-46.
2. Oudenhoven, J.F.M., Baggetto, L. and Notten, P.H.L., *All-Solid-State Lithium-Ion Microbatteries: A Review of Various Three-Dimensional Concepts.* Advanced Energy Materials, 2011. **1**(1): p. 10-33.
3. Wang, Y., et al., *Lithium and lithium ion batteries for applications in microelectronic devices: A review.* Journal of Power Sources, 2015. **286**: p. 330-345.
4. Roberts, M., et al., *3D lithium ion batteries—from fundamentals to fabrication.* Journal of Materials Chemistry, 2011. **21**(27): p. 9876.
5. Arthur, T.S., et al., *Three-dimensional electrodes and battery architectures.* MRS Bulletin, 2011. **36**(07): p. 523-531.
6. Bates, J., et al., *Thin-film lithium and lithium-ion batteries.* Solid State Ionics, 2000. **135**(1): p. 33-45.
7. Long, J.W., et al., *Three-Dimensional Battery Architectures.* Chemical Reviews, 2004. **104**(10): p. 4463-4492.
8. Nathan, M., et al., *Three-dimensional thin-film Li-ion microbatteries for autonomous MEMS.* Microelectromechanical Systems, Journal of, 2005. **14**(5): p. 879-885.
9. Liu, C., et al., *An all-in-one nanopore battery array.* Nat Nanotechnol, 2014. **9**(12): p. 1031-9.
10. Gowda, S.R., et al., *Building energy storage device on a single nanowire.* Nano Lett, 2011. **11**(8): p. 3329-33.
11. Pikul, J.H., et al., *High-power lithium ion microbatteries from interdigitated three-dimensional bicontinuous nanoporous electrodes.* Nat Commun, 2013. **4**: p. 1732.
12. Gowda, S.R., et al., *3D nanoporous nanowire current collectors for thin film microbatteries.* Nano Lett, 2012. **12**(3): p. 1198-202.

13. Sun, K., et al., *3D printing of interdigitated Li-ion microbattery architectures.* Adv Mater, 2013. **25**(33): p. 4539-43.

14. Cheah, S.K., et al., *Self-supported three-dimensional nanoelectrodes for microbattery applications.* Nano Lett, 2009. **9**(9): p. 3230-3.

15. Wang, C., et al., *C-MEMS for the Manufacture of 3D Microbatteries.* Electrochemical and Solid-State Letters, 2004. **7**(11): p. A435.

16. Min, H.-S., et al., *Fabrication and properties of a carbon/polypyrrole three-dimensional microbattery.* Journal of Power Sources, 2008. **178**(2): p. 795-800.

17. Kotobuki, M., et al., *Fabrication of Three-Dimensional Battery Using Ceramic Electrolyte with Honeycomb Structure by Sol–Gel Process.* Journal of The Electrochemical Society, 2010. **157**(4): p. A493.f

18. Zhang, J., et al., *Honeycomb-like porous gel polymer electrolyte membrane for lithium ion batteries with enhanced safety.* Sci Rep, 2014. **4**: p. 6007.

19. Lethien, C., et al., *Micro-patterning of LiPON and lithium iron phosphate material deposited onto silicon nanopillars array for lithium ion solid state 3D micro-battery.* Microelectronic Engineering, 2011. **88**(10): p. 3172-3177.

20. Tan, S., et al., *A solid state 3-D microbattery based on Cu2Sb nanopillar anodes.* Solid State Ionics, 2012. **225**: p. 510-512.

21. Tan, S., et al., *3-D microbattery electrolyte by self-assembly of oligomers.* Solid State Ionics, 2011. **198**(1): p. 26-31.

22. Delannoy, P.E., et al., *Toward fast and cost-effective ink-jet printing of solid electrolyte for lithium microbatteries.* Journal of Power Sources, 2015. **274**: p. 1085-1090.

23. Xu, K., *Nonaqueous Liquid Electrolytes for Lithium-Based Rechargeable Batteries.* Chemical Reviews, 2004. **104**(10): p. 4303-4418.

24. Roth, E.P. and Orendorff, C.J., *How electrolytes influence battery safety.* 2012.

25. Garcia, B., et al., *Room temperature molten salts as lithium battery electrolyte.* Electrochimica Acta, 2004. **49**(26): p. 4583-4588.

26. Holzapfel, M., Jost, C. and Novak, P., *Stable cycling of graphite in an ionic liquid based electrolyte.* Chem Commun (Camb), 2004(18): p. 2098-9.

27. Seki, S., et al., *Lithium secondary batteries using modified-imidazolium room-temperature ionic liquid.* J Phys Chem B, 2006. **110**(21): p. 10228-30.

28. Jayathilaka, P.A.R.D., et al., *Effect of nano-porous Al2O3 on thermal, dielectric and transport properties of the (PEO)9LiTFSI polymer electrolyte system.* Electrochimica Acta, 2002. **47**(20): p. 3257-3268.

29. Vallée, A., Besner, S. and Prud'Homme, J., *Comparative study of poly(ethylene oxide) electrolytes made with LiN(CF3SO2)2, LiCF3SO3 and LiClO4: Thermal properties and conductivity behaviour.* Electrochimica Acta, 1992. **37**(9): p. 1579-1583.

30. Edman, L., *Ion Association and Ion Solvation Effects at the Crystalline−Amorphous Phase Transition in PEO−LiTFSI.* The Journal of Physical Chemistry B, 2000. **104**(31): p. 7254-7258.

31. Gorecki, W., et al., *Physical properties of solid polymer electrolyte PEO(LiTFSI) complexes.* Journal of Physics: Condensed Matter, 1995. **7**(34): p. 6823-6832.

32. Song, J.Y., Wang, Y.Y. and Wan, C.C., *Review of gel-type polymer electrolytes for lithium-ion batteries.* Journal of Power Sources, 1999. **77**(2): p. 183-197.

33. Quartarone, E. and Mustarelli, P., *Electrolytes for solid-state lithium rechargeable batteries: recent advances and perspectives.* Chem Soc Rev, 2011. **40**(5): p. 2525-40.

34. Ito, Y., et al., *Ionic conductivity of electrolytes formed from PEO-LiCF3SO3 complex low molecular weight poly(ethylene glycol).* Journal of Materials Science, 1987. **22**(5): p. 1845-1849.

35. Kelly, I.E., Owen, J.R. and Steele, B.C.H., *Poly(Ethylene Oxide) Electrolytes for Operation at near Room-Temperature.* Journal of Power Sources, 1985. **14**(1-3): p. 13-21.

36. Fergus, J.W., *Ceramic and polymeric solid electrolytes for lithium-ion batteries.* Journal of Power Sources, 2010. **195**(15): p. 4554-4569.

37. Fan, L.-Z., et al., *Enhanced ionic conductivities in composite polymer electrolytes by using succinonitrile as a plasticizer.* Solid State Ionics, 2008. **179**(27-32): p. 1772-1775.

38. Itoh, T., et al., *Solid polymer electrolytes based on squaric acid structure.* Ionics, 2007. **14**(1): p. 1-6.

39. Agrawal, R.C. and Pandey, G.P., *Solid polymer electrolytes: Materials designing and all-solid-state battery applications: An overview.* Journal of Physics D: Applied Physics, 2008. **41**(22).

40. Pitawala, H.M.J.C., et al., *Effect of plasticizers (EC or PC) on the ionic conductivity and thermal properties of the (PEO)9LiTf: Al2O3 nanocomposite polymer electrolyte system.* Journal of Solid State Electrochemistry, 2008. **12**(7-8): p. 783-789.

41. Skaarup, S., *Mixed phase solid electrolytes.* Solid State Ionics, 1988. **28-30**: p. 975-978.

42. Wieczorek, W., *Temperature dependence of conductivity of mixed-phase composite polymer solid electrolytes.* Materials Science and Engineering: B, 1992. **15**(2): p. 108-114.

43. Liu, Y., Lee, J.Y. and Hong, L., *Functionalized SiO2 in poly(ethylene oxide)-based polymer electrolytes.* Journal of Power Sources, 2002. **109**(2): p. 507-514.

44. Wang, X.-L., et al., *Polymer composite electrolytes containing ionically active mesoporous SiO[sub 2] particles.* Journal of Applied Physics, 2007. **102**(5): p. 054907.

45. Croce, F., Settimi, L. and Scrosati, B., *Superacid ZrO2-added, composite polymer electrolytes with improved transport properties.* Electrochemistry Communications, 2006. **8**(2): p. 364-368.

46. Forsyth, M., *The effect of nano-particle TiO2 fillers on structure and transport in polymer electrolytes.* Solid State Ionics, 2002. **147**(3-4): p. 203-211.

47. Croce, F., *Nanocomposite polymer electrolytes and their impact on the lithium battery technology.* Solid State Ionics, 2000. **135**(1-4): p. 47-52.

48. Tarascon, J.M., et al., *Performance of Bellcore's plastic rechargeable Li-ion batteries.* Solid State Ionics, 1996. **86-88**: p. 49-54.

49. Ren, Z., et al., *Polymer electrolytes based on poly(vinylidene fluoride-co-hexafluoropropylene) with crosslinked poly(ethylene glycol) for lithium batteries.* Solid State Ionics, 2009. **180**(9-10): p. 693-697.

50. Kuo, C.W., et al., *Enhanced Ionic Conductivity in PAN-PEGME-LiClO4-PC Composite Polymer Electrolytes.* International Journal of Electrochemical Science, 2013. **8**(3): p. 3834-3850.

51. Patel, M., Chandrappa, K.G. and Bhattacharyya, A.J., *Increasing ionic conductivity and mechanical strength of a plastic electrolyte by inclusion of a polymer.* Electrochimica Acta, 2008. **54**(2): p. 209-215.

52. Perera, K.S., et al., *Application of polyacrylonitrile-based polymer electrolytes in rechargeable lithium batteries.* Journal of Solid State Electrochemistry, 2007. **12**(7-8): p. 873-877.

53. Li, Q. and Ardebili, H., *Flexible thin-film battery based on solid-like ionic liquid-polymer electrolyte.* Journal of Power Sources, 2016. **303**: p. 17-21.

54. Gaikwad, A.M., Arias, A.C. and Steingart, D.A., *Recent Progress on Printed Flexible Batteries: Mechanical Challenges, Printing Technologies, and Future Prospects.* Energy Technology, 2015. **3**(4): p. 305-328.

55. Kwon, Y.H., et al., *Cable-type flexible lithium ion battery based on hollow multi-helix electrodes.* Adv Mater, 2012. **24**(38): p. 5192-7, 5145.

56. Koo, M., et al., *Bendable inorganic thin-film battery for fully flexible electronic systems.* Nano Lett, 2012. **12**(9): p. 4810-6.

57. Liu, B., et al., *Hierarchical three-dimensional ZnCo(2)O(4) nanowire arrays/carbon cloth anodes for a novel class of high-performance flexible lithium-ion batteries.* Nano Lett, 2012. **12**(6): p. 3005-11.

58. Ho, C.C., et al., *A super ink jet printed zinc–silver 3D microbattery.* Journal of Micromechanics and Microengineering, 2009. **19**(9): p. 094013.

59. Kil, E.H., et al., *Imprintable, bendable, and shape-conformable polymer electrolytes for versatile-shaped lithium-ion batteries.* Adv Mater, 2013. **25**(10): p. 1395-400.

60. Xue, Z., et al., *High-Speed Fabrication of Lithium-Ion Battery Electrodes by UV-Curing.* Energy Technology, 2015. **3**(5): p. 469-475.

61. Rahimi, M., et al., *Effects of aluminium surface morphology and chemical modification on wettability.* Applied Surface Science, 2014. **296**: p. 124-132.

62. Kim, S.H., et al., *Printable Solid-State Lithium-Ion Batteries: A New Route toward Shape-Conformable Power Sources with Aesthetic Versatility for Flexible Electronics.* Nano Lett, 2015. **15**(8): p. 5168-77.

63. Polu, A.R., et al., *Effect of TiO[sub 2] ceramic filler on PEG-based composite polymer electrolytes for magnesium batteries.* 2013: p. 996-997.

64. Mogurampelly, S. and Ganesan, V., *Effect of Nanoparticles on Ion Transport in Polymer Electrolytes.* Macromolecules, 2015. **48**(8): p. 2773-2786.

65. Ji, K.-S., et al., *Role of functional nano-sized inorganic fillers in poly(ethylene) oxide-based polymer electrolytes.* Journal of Power Sources, 2003. **117**(1-2): p. 124-130.

66. Weston, J. and Steele, B., *Effects of inert fillers on the mechanical and electrochemical properties of lithium salt-poly(ethylene oxide) polymer electrolytes.* Solid State Ionics, 1982. **7**(1): p. 75-79.

67. Kim, W., et al., *Study on cycling performances of lithium-ion polymer cells assembled by in situ chemical cross-linking with star-shaped siloxane acrylate.* Journal of Power Sources, 2008. **178**(2): p. 837-841.

68. Kang, Y., et al., *Solid polymer electrolytes based on cross-linked polysiloxane-g-oligo(ethylene oxide): ionic conductivity and electrochemical properties.* Journal of Power Sources, 2003. **119-121**: p. 448-453.

APPENDIX

APPENDIX

The active material LFP is mixed with PEG resin to form an electrode resin. It is cured by UV laser writer, as shown in Figure A-1. The laser power is so strong that it 'draws' a line wider than its actual width, because the electrode resin near the region is also cured by the heat. The patterns also influence the shape integrity to the electrode's microstructure. For the left pattern in Figure A-1, it has a better integrity because its network shape and wider lines. Compared with that, the right pattern is deformed after treating with UV laser writer and it also detached from the substrate. The cured electrode resin is then baked at high temperature to pyrolysis the PEG. However, during the heating process the LFP is oxidized and turned into red. This is due to the residue oxygen left in the oven and the electrode resin.

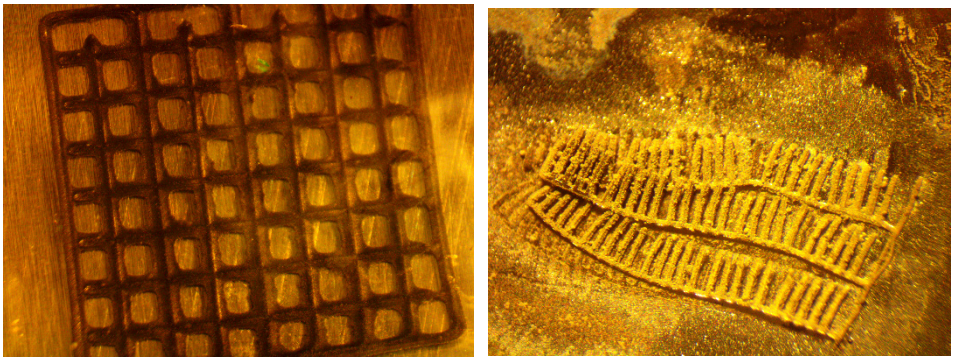

Figure A-1. LFP powder and PEG resin mixture patterned by UV laser writer.